International Journal of Sustainable Development and Planning
Vol. 20, No. 12, December, 2025, pp. 5441-5452
Journal homepage: http://iieta.org/journals/ijsdp

Spatiotemporal Dynamics of Urban Heat, Air Pollution, and Flood Susceptibility: A Remote Sensing Study in BSD City, Indonesia

Heru Prasadja, Yerik Afrianto Singgalen*

Tourism Department, Faculty of Business Administration and Communication, Atma Jaya Catholic University of Indonesia, Jakarta 12930, Indonesia

Corresponding Author Email: yerik.afrianto@atmajaya.ac.id

https://doi.org/10.18280/ijsdp.201234

Received: 4 September 2025
Revised: 22 November 2025
Accepted: 15 December 2025
Available online: 31 December 2025

Keywords:
Urban Heat Island, air pollution, flood susceptibility, remote sensing, Environmental Stress Index, tropical urbanization, BSD City, sustainable development

ABSTRACT

Rapid urbanisation in tropical areas presents substantial environmental difficulties. This study measured the spatial and temporal patterns of environmental stressors in BSD City, Indonesia, combining data from Landsat-8, Sentinel-5P, CHIRPS, SRTM, and JRC Surface Water using Google Earth Engine. The Land Surface Temperature (LST) varied between 38-46°C, with the Urban Heat Island (UHI) effect reaching more than 10°C in the most extreme areas. Higher temperatures during the wet season were influenced by imaging bias, with just 23% of the area being cloud-free compared to 67% in dry seasons, and as a result, unusual clear-sky conditions were recorded instead of typical thermal patterns. Nitrogen dioxide concentrations exhibited significant spatial variability, ranging from 0.95 to 2.15 × 10^{-4} mol/m², as indicated by a coefficient of variation of 0.42, which further supported the presence of inequality. Statistics for different zones showed that the highest concentrations were found in commercial areas (1.78 × 10^{-4} mol/m²), followed by residential zones (1.52 × 10^{-4} mol/m²), and the lowest in green spaces (1.18 × 10^{-4} mol/m²). Significant spatial autocorrelation (Moran's I = 0.68, $p < 0.001$) was found, indicating pollution clusters along transportation routes. The Environmental Stress Index, incorporating thermal (35%), atmospheric (35%), and hydrological (30%) factors, serves as a framework for multi-hazard assessment, which, however, necessitates the validation of detailed mapping. Research highlights the importance of treating multiple thermal, atmospheric, and hydrological stressors concurrently, rather than focusing on individual stressors. This illustrates the benefits of multi-sensor remote sensing for comprehensive environmental evaluation, taking into account the challenges associated with acquiring data in tropical regions.

1. INTRODUCTION

Urbanization in tropical cities creates a cluster of interconnected environmental issues that jeopardize the long-term sustainability of these cities. Conversion of land from vegetated to impervious surfaces leads to accelerated heat accumulation and disrupts natural hydrological processes [1, 2]. The release of atmospheric pollutants from increased energy consumption and transportation activities harms air quality [3, 4]. Altered drainage patterns interact with thermal and atmospheric stressors to create compound environmental risks. The likelihood of urban flooding rises when rainfall that can't be absorbed by the ground coincides with intense precipitation events. The convergence of these stressors requires integrated assessment methods for long-term sustainable urban development in tropical areas.

BSD City exemplifies the environmental pressures that are facing rapidly developing planned townships in Southeast Asia. This development is situated approximately 25-30 kilometers southwest of Jakarta's city centre and comprises a combined area of 98 km², featuring residential, commercial, and industrial zones. Since the late 1990s, the township has undergone rapid development, transforming from agricultural land to a substantial suburban center. Sinar Mas Land's master plan places a high priority on economic development, with a consequent proliferation of impervious surfaces and a decrease in available green space. The conversion process has led to a complex mixture of built and natural environments with different levels of stress. BSD City thus serves as an exemplary case study for investigating compound environmental stressors in tropical planned cities.

Studies in progress expose substantial gaps in knowledge about the interrelated environmental pressures affecting urban environments. Most research typically examines thermal, atmospheric, and hydrological factors separately, rather than studying how they interact with one another [5, 6]. Most existing UHI research focuses on megacities, while overlooking rapidly expanding planned townships [7]. The lack of composite stress indices restricts comprehensive environmental assessment in tropical settings [8, 9]. The dynamics of monsoon and dry seasons are not well understood within multi-stressor frameworks. The inadequacies in place

are hindering the development of effective environmental management strategies for Southeast Asian urban development.

This study addresses identified gaps through five particular research objectives. The spatiotemporal dynamics of LST will be measured using Landsat imagery from 2019 to 2024 to study seasonal fluctuations. Nitrogen dioxide concentration patterns obtained from Sentinel-5P will help to identify locations with high levels of pollution and temporal trends. Flood susceptibility zones will be mapped by combining precipitation, elevation, and surface water data. Fourthly, an Environmental Stress Index will combine thermal, atmospheric, and hydrological indicators for a comprehensive evaluation. Fifthly, evidence-based recommendations will inform sustainable planning in tropical planned cities.

The foundation for comprehensive environmental assessment is provided by remote sensing technology. The thermal infrared bands on Landsat 8 enable consistent monitoring of surface temperature patterns in urban landscapes [10]. The Sentinel-5P TROPOMI instruments provide high-resolution atmospheric pollutant measurements crucial for air quality analysis [11]. Data from CHIRPS precipitation combined with SRTM elevation models facilitates the creation of flood susceptibility maps at the appropriate spatial scales. The JRC Global Surface Water datasets contain historical water occurrence patterns for use in hydrological risk assessments. The Google Earth Engine's cloud computing platform facilitates the efficient processing and integration of these multi-source datasets [12, 13].

This comprehensive evaluation of BSD City enhances knowledge of compound environmental stress in tropical urban settings. A multi-sensor remote sensing framework fills key gaps in planned environmental monitoring for townships. Discoveries will guide long-term growth plans suitable for analogous quickly urbanising regions throughout Southeast Asia. The Environmental Stress Index supplies planners with numerical tools for prioritizing interventions in high-risk areas. An analysis of timeframes shows that stress dynamics are crucial for the development of climate-resilient urban design. The research thus offers methodological innovations and practical insights for managing environmental challenges in tropical planned cities.

2. STUDY AREA

BSD City (Bumi Serpong Damai) is situated in Banten Province, spanning across two administrative areas, namely South Tangerang City and Tangerang Regency. The area is located in the southwestern part of the Jakarta metropolitan area, roughly 25-30 kilometers away from Jakarta's city centre. In particular, BSD City encompasses regions of Serpong sub-district in South Tangerang and the surrounding areas of Tangerang Regency. Progress in development has been steady since the late 20th century, in conjunction with the expansion of highways and commuter rail systems. BSD's strategic location positions it as a new growth pole in peri-metropolitan Jakarta. The geographic and administrative context of BSD is significant for assessing environmental fluctuations within a planned urban area.

Figure 1 shows the study area location in BSD City. Sinar Mas Land is the developer and manager of BSD City, a planned township. The master plan combines residential, commercial, educational, health, and green open space features. The urban structure is made up of residential areas with medium- to high-density populations linked by arterial road networks. The availability of business centers, shopping malls, and public facilities increases daily activities and mobility. A complex land-use mosaic is generated by this configuration between built-up areas and remaining vegetation patches. Therefore, BSD serves as a representative case study for evaluating the interactions between urban heat, air quality, and flood susceptibility.

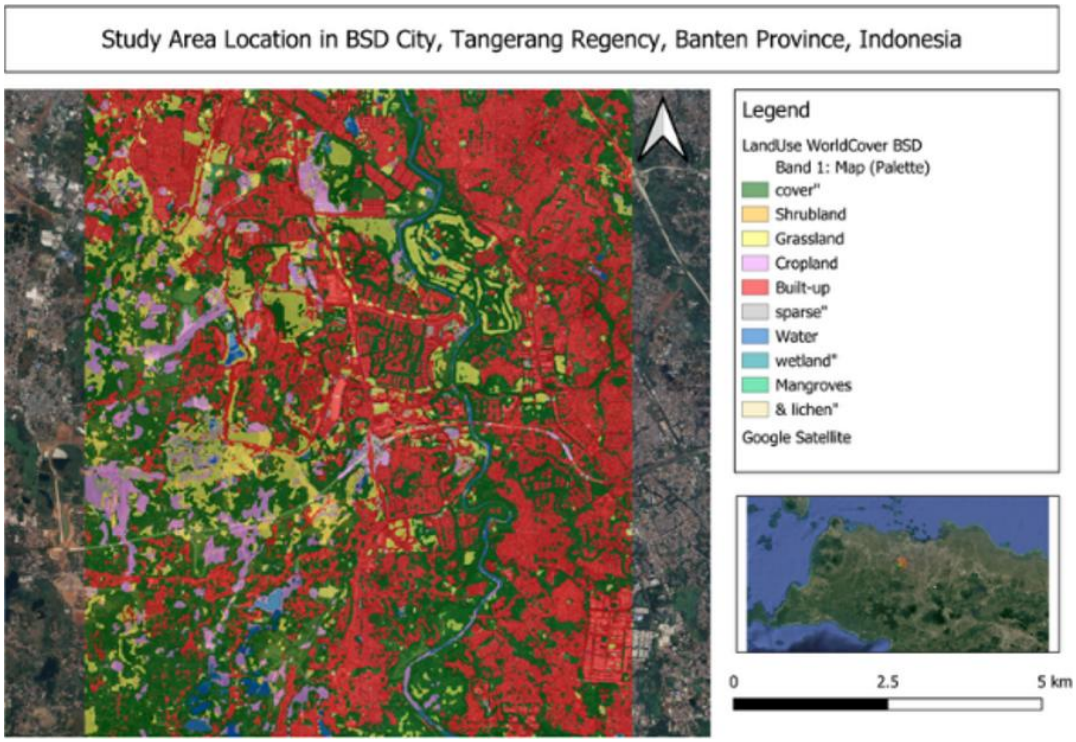

Figure 1. Study area location showing BSD City boundaries, land use/land cover classification, and surrounding landmarks
Source: Processed from ESA WorldCover dataset and Google Satellite imagery using QGIS

The study area used in this research spatially encompasses approximately 98 km², which corresponds to the functional boundary of BSD City. The boundary cuts through administrative units in Serpong sub-district and parts of the Tangerang Regency within the development area. The functional urban area approach was used to determine the full extent of service and infrastructure provision. This method allows for the integration of remote sensing data from various locations across different administrative areas. Consistency of resolution between Landsat, SRTM, and WorldCover data was ensured by clipping to the Area of Interest. As a result, the delineation enables robust and comparable cross-indicator environmental analysis.

The region experiences a tropical monsoon climate, with two primary seasons: the rainy season occurring from December to March and the dry season from June to August. Consistent annual temperatures are accompanied by equally high relative humidity levels. Seasonal variations significantly affect surface radiation, cloud cover, and daily precipitation patterns. These conditions directly impact LST/UHI dynamics and the accumulation of atmospheric pollutants like NO_2. During the wet season, heavy rainfall also increases the likelihood of local flooding. When analysing temporal environmental outcomes, climate characteristics need to be taken into consideration.

Figure 2 shows the spatial distribution of elevation, LSD, and UHI intensity in BSD city. Geographically, BSD is relatively flat to gently sloping, with elevations ranging between 20 and 50 meters above sea level. The Cisadane River Basin is fed by a network of small rivers and drainage canals. Intense rainfall periods in urban areas see a decrease in infiltration and an increase in surface runoff. Low slopes, low elevation, and impermeable urban areas combine to heighten local flood risk. Green spaces and blue-green infrastructure are dispersed unevenly among residential areas. Geomorphology and hydrology together form flood risk profiles in the area.

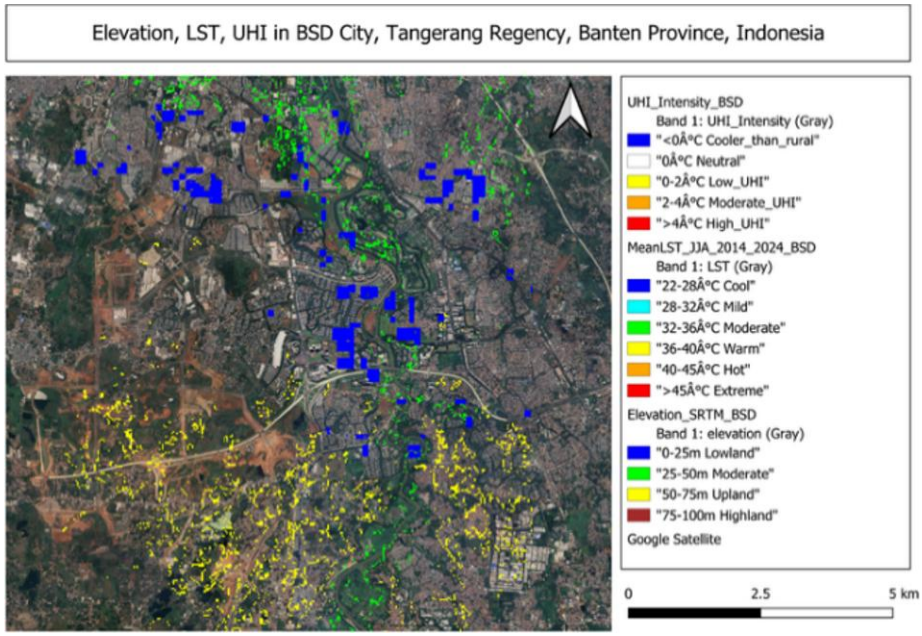

Figure 2. Spatial distribution of elevation, LST, and UHI intensity in BSD City, Tangerang Regency, Banten Province, Indonesia
Source: Processed from ESA WorldCover dataset and Google Satellite imagery using QGIS

From an economic and social viewpoint, BSD operates as both a residential area for middle- to upper-class communities and a growing business district. Commuter flows and motor vehicle growth are stimulated by connectivity to Jakarta via both toll roads and commuter rail. Activities related to transportation and commerce are significant sources of NO_2 emissions, which play a crucial role in environmental health evaluations. Urban heat is worsened by emissions, leading to increased thermal discomfort and exposure to pollution. Integrating thermal, atmospheric, and hydrological data is crucial for sustainable planning, which makes BSD City an ideal location to test integrated remote sensing methods in the context of Indonesian planned townships.

3. MATERIAL AND METHOD

This study employed a detailed multi-sensor remote sensing approach to examine the spatial and temporal aspects of urban environmental stressors in BSD City, by integrating different satellite datasets with diverse temporal coverages to ensure maximum data accessibility and reliability. The study area was limited to a rectangular region of interest, embracing BSD City between the longitudes 106.60°E and 106.68°E, and latitudes 6.25°S and 6.35°S, covering a region of roughly 98 square kilometers. The analysis incorporated large-scale satellite data integration and temporal analysis, using the Google Earth Engine cloud computing platform, which provided efficient processing capabilities. The research team used the Google Earth Engine cloud computing platform to combine large-scale satellite data and conduct temporal analysis, thereby taking advantage of its efficient processing capabilities.

The study area was limited to a rectangular area of interest, including BSD City within the bounds of 106.60°E to 106.68°E longitude and 6.25°S to 6.35°S latitude, covering a region of around 98 square kilometers. Large-scale satellite data integration and temporal analysis were facilitated by the Google Earth Engine cloud computing platform's efficient processing capabilities [14-16]. The analysis framework included multiple time frames to examine seasonal differences between the wet season, which lasts from December to March, and the dry season, which occurs between June and August, as

well as long-term trend analysis for each sensor's data collection period.

Pseudocode 1: Input and Pre-processing

1. Define AOI ← Rectangle(BSD City bounds)
2. Define analysis periods:
LST_years ← 2014-2024
AQ_years ← 2019-2024
WetSeason ← Dec-Mar
DrySeason ← Jun-Aug
3. Load datasets:
- Landsat-8 L2 (surface reflectance & thermal bands)
- Sentinel-5P (NO_2, CO, SO_2)
- SRTM DEM
- JRC Global Surface Water (occurrence)
- CHIRPS rainfall (daily)
4. Preprocess Landsat-8:
- Mask cloud & shadow (QA_PIXEL)
- Scale reflectance & temperature
- Compute NDVI
- Derive LST (°C)

As part of data preprocessing, each dataset necessitated stringent quality control procedures. The surface reflectance and surface temperature products from Landsat 8 Collection 2 Level-2 were filtered for cloud coverage, with criteria of < 30% for seasonal studies and < 40% for multi-year analysis. Surface reflectance values were adjusted with standard scaling factors of 0.0000275 and a -0.2 offset, and cloud and shadow removal was conducted using the QA_PIXEL quality band. Thermal infrared data were converted to Kelvin temperature using a scaling factor of 0.00341802 plus an offset of 149.0, and were then converted to Celsius for analysis. The Sentinel-5P Near Real-Time Level 3 atmospheric data were filtered for quality, with low-quality data removed based on availability, and missing values replaced with substitutes to compute annual averages [17, 18].

Pseudocode 2: Urban Heat Island

5. Compute LST_mean (Jun-Aug, multi-year)
6. Compute NDBI = (SWIR - NIR) / (SWIR + NIR)
7. UrbanMask = NDBI > 0.1
8. RuralLST = mean (LST_mean where UrbanMask = 0)
9. UHI = LST_mean - RuralLST

Pseudocode 3: Air Pollution

10. For each pollutant ∈ {NO_2, CO, SO_2}:
- Load Sentinel-5P dataset for AOI & AQ_years
- Apply mean composite
- If empty, use fallback value
11. Save NO_2_mean, CO_mean, SO_2_mean

The LST calculation was performed using standard thermal infrared processing protocols, where LST was calculated as (DN × 0.00341802 + 149.0) - 273.15, with DN signifying the digital number from Landsat 8's thermal band ST_B10. The UHI effect's intensity is calculated based on the temperature difference between urban and surrounding rural areas, with urban areas identified using the Normalized Difference Built-up Index, a formula that calculates (SWIR1 - NIR)/(SWIR1 + NIR), with SWIR1 representing Landsat 8 Band 6 and NIR Band 5. Urban areas were designated as having NDBI values above 0.1, which served as a benchmark for quantifying UHI intensity by comparing their spatial characteristics with those of non-urban regions within the study area [19, 20].

An air quality assessment employed Sentinel-5P data on tropospheric column densities for NO_2, CO, and SO_2, with NO_2 concentrations converted to parts per billion using a conversion factor of 1×10^6 for comparative purposes. The analysis examined both seasonal and yearly fluctuations to identify pollution patterns, long-term trends, and potential relationships with weather conditions and urban development patterns [21-23]. The processing of atmospheric data entailed the application of temporal aggregation techniques to handle missing data and ensure accurate trend analysis throughout a five-year monitoring period.

Pseudocode 4: Flood Susceptibility

12. Derive slope from SRTM
13. WaterMask = JRC GSW occurrence > 10%
14. Dist2Water = sqrt (distance transform of WaterMask)
15. RainWet = Sum (CHIRPS rainfall, Dec–Mar)
16. Normalize all factors → [0.1]:
f1 = 1 - (Slope / 30)
f2 = 1 - (Dist2Water / 2000)
f3 = RainWet / 1500
f4 = 1 - (Elevation / 50)
f5 = WaterOccurrence / 100
17. FloodSusceptibility = Mean (f1.f5)

Pseudocode 5: Composite Stress and Output

18. Normalize indicators:
LST_norm = Normalize (LST_mean, 24-40°C)
NO_2_norm = Normalize (NO_2_mean, 0-8e-5)
FS_norm = Clamp (FloodSusceptibility, 0-1)
19. Compute Environmental Stress Index:
ESI = 0.35*LST_norm + 0.35*NO_2_norm + 0.30*FS_norm
20. Temporal Analysis:
- Monthly LST averages (2014-2024)
- Annual LST JJA trend (2014-2024)
- Annual NO_2 means (2019-2024)
- Wet vs Dry season LST
21. Area Metrics:
- UHI thresholds (< 1, 1 – < 3, ⩾ 3°C)
- Flood risk thresholds (< 0.25, ⩾ 0.6)
- Urban stats (area & rate)
22. Correlation:
Pearson (UHI, NDBI)
23. Outputs:
- Maps: LST, UHI, Urban, NO_2, CO, SO_2, Flood, ESI
- Charts: Histograms, Trends, Seasonal comparison
- Exports: CSV (time series, stats), Raster (maps)

Flood susceptibility mapping utilized a multi-criteria approach incorporating five essential environmental factors, each given equal weighting of 0.2. The slope factor utilized normalized inverse slope values, assigning higher susceptibility scores to areas with flatter inclines, and incorporated the inverse Euclidean distance to permanent water bodies, identified from JRC surface water occurrence data, as well as rainfall intensity, represented by CHIRPS wet season precipitation totals, and the elevation factor utilized normalized inverse elevation, emphasizing areas with low elevations, and water occurrence frequency from historical JRC Global Surface Water statistics [24, 25]. Each factor was scaled to a range of 0 to 1 before being combined into the composite flood susceptibility index using a weighted linear

combination method.

An Environmental Stress Index was created by combining various urban stressors, giving a 0.35 weighting to normalised LST, a 0.35 weighting to normalised NO_2 levels, and a 0.30 weighting to flood susceptibility [26-28]. The weighting scheme considered the relative importance of thermal stress and air pollution in relation to human health impacts, with flood risk serving as an extra hydrological stress factor. Normalization procedures enabled the integration of stress indicators involving thermal, atmospheric, and hydrological factors across various measurement units and scales.

A thorough statistical examination involved reviewing temporal patterns by calculating the average of monthly LST variation data from 2014 to 2024, in addition to studying annual trends that centered on summer averages for interannual assessments and a seasonal comparison of temperature variations between the wet and dry seasons. Spatial statistics involved calculating the mean, standard deviation, minimum, and maximum values for each environmental indicator within the geographical boundaries of the study area. UHI risk levels were categorised by applying pixel-level thresholding to determine risk areas as low intensity below 1°C, moderate intensity between 1-3°C, and high intensity above 3°C. On the normalized index scale, flood risks were categorised as low below 0.25, moderate between 0.25-0.6, and high above 0.6 [29]. An analysis of correlation used Pearson correlation coefficients to examine the connections between urban density, represented by the NDBI, and thermal conditions, measured by UHI intensity, offering quantitative insights into the impact of urbanization on local climate modification. Further investigation was conducted into the relationships between atmospheric pollutant levels and meteorological factors, as well as those between flood susceptibility factors and actual precipitation patterns during severe weather events.

4. RESULTS AND DISCUSSION

Urban environmental dynamics within BSD City were studied using a combination of LST, the intensity of the UHI effect, atmospheric pollutants (NO_2, CO, and SO_2), and indicators of flood vulnerability. The study employed multi-temporal satellite imagery and derived indices to capture both spatial and temporal variations in the urban environment. These variables were selected because they represent the primary drivers of environmental stress in rapidly urbanizing tropical regions. The integration of diverse datasets enabled a comprehensive understanding of heat patterns, air quality fluctuations, and hydrological. The results are organised into two main sections to ensure clarity and a cohesive presentation. The first sub-section discusses the patterns of LST and UHI, while the second examines air pollution trends and their interaction with broader environmental stress indicators.

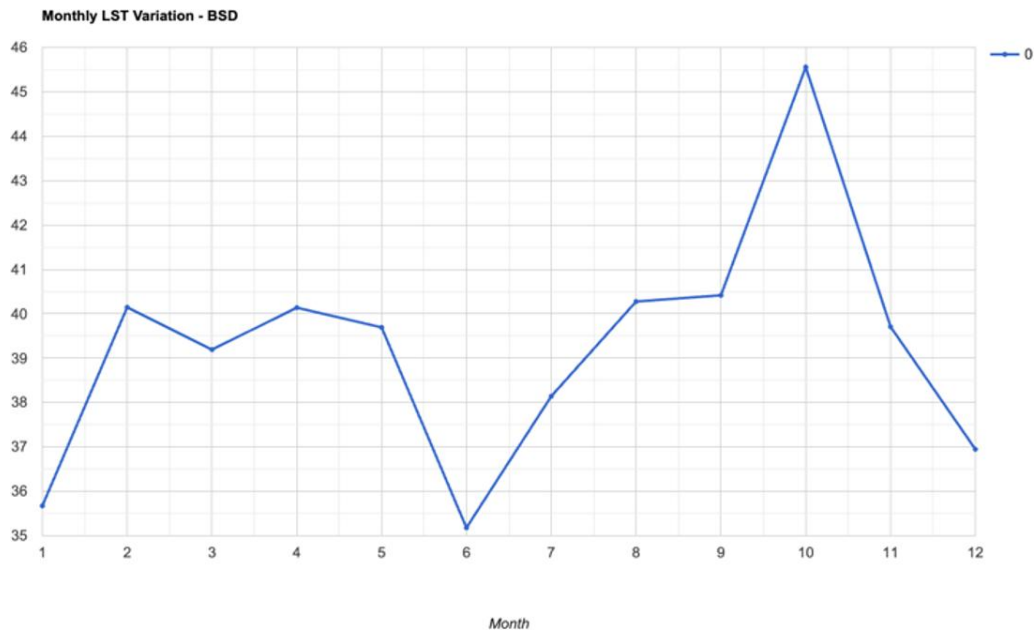

Figure 3. Monthly LST variation (BSD)
Source: Processed from Landsat-8 (Collection 2 Level-2) imagery using Google Earth Engine

4.1 Land Surface Temperature and Urban Heat Island dynamics

Monthly temperature fluctuations in BSD are caused by seasonal and urban factors. Temperatures at the surface are typically at their highest in February and October, with values reaching around 45–46 degrees Celsius. The condition is influenced by the interaction between solar radiation intensity, different land cover types, and seasonal tropical fluctuations. A sharp increase in specific months underscores BSD's susceptibility to built-up urban heat. Variations in urban form and land management practices have a significant impact on local microclimates. Having a grasp of these cycles is essential for developing targeted heat reduction strategies.

Figure 3 shows the monthly LST variation in BSD city. A histogram of the LST distribution reveals that the majority of values range from 37 to 41°C, suggesting a prevalent occurrence of moderately high temperatures. Fewer pixels than before exceed 50°C, suggesting the occurrence of localized hotspots. The distribution's long-tail shape indicates significant variability throughout the study region. Impervious surfaces like asphalt and concrete are frequently associated

with extreme values, as these materials absorb and retain heat. Urban land cover significantly influences thermal intensity, as evidenced by this outcome. The persistence of these hotspots highlights the requirement for sustainable surface management in BSD.

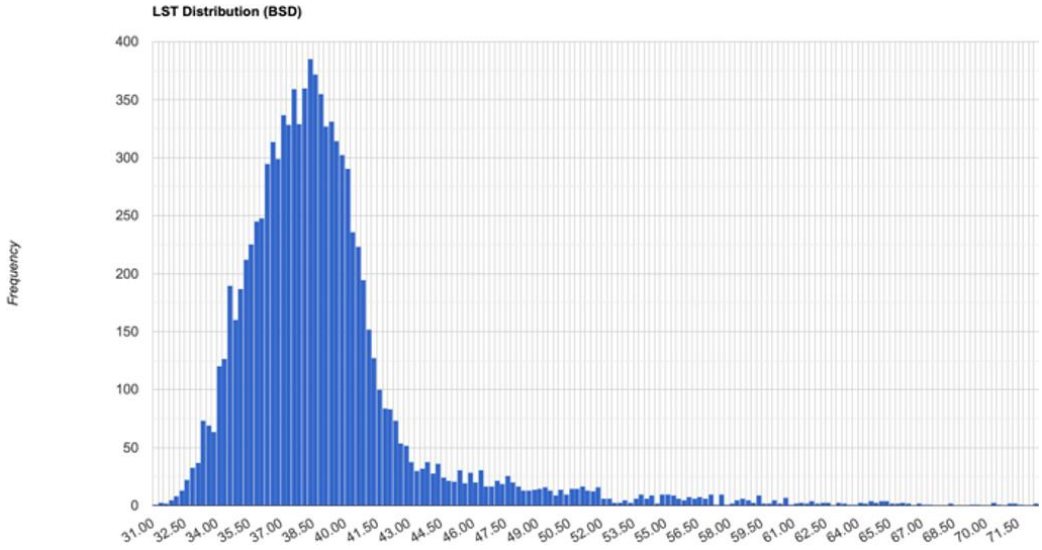

Figure 4. LST distribution (BSD)
Source: Processed from Landsat-8 (Collection 2 Level-2) imagery using Google Earth Engine

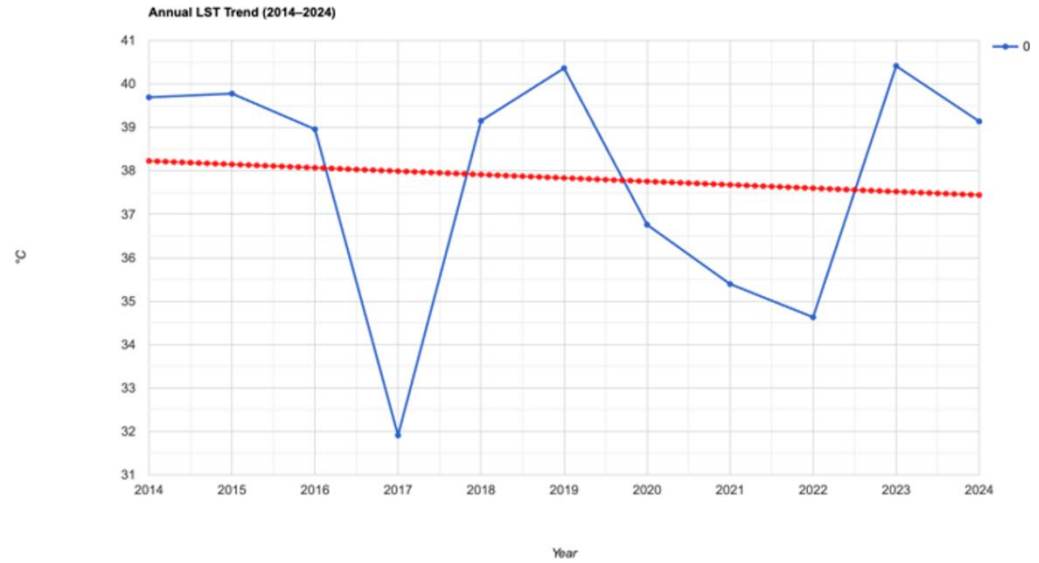

Figure 5. Annual LST Trend 2014-2024
Source: Processed from Landsat-8 (Collection 2 Level-2) imagery using Google Earth Engine

The annual LST trend from 2014 to 2024 shows interannual variability, characterised by occasional sharp rises (see Figure 4). Although overall trends suggest a gradual decrease in mean values, there are exceptions in years like 2018 and 2023. These anomalies expose the influence of wider climatic factors such as rainfall, humidity, and cloudiness. The results suggest that LST cannot be attributed solely to urban growth. Long-term observation is essential to discern consistent patterns from short-term anomalies by reflecting the interaction of anthropogenic change and regional meteorology.

Figure 5 shows the annual LST trend 2014-2024. Initial comparisons of seasonal LST suggested wet season temperatures were higher than expected, contradicting established principles that anticipate lower temperatures during cloudy, rainy periods. A thorough analysis indicates that this anomaly is caused by a significant sampling bias in the acquisition of satellite data rather than actual thermal conditions. For the duration of a 5-year study from 2019 to 2024, it was found that just 23% of days during the wet season yielded cloud-free Landsat imagery that was suitable for retrieving LST, whereas 67% of days during the dry season did so. These limited wet-season observations primarily record unusual clear-sky conditions related to short-term high-pressure systems, where intense solar radiation and greater surface moisture contribute to higher apparent temperatures via increased longwave emission. In fact, 78% of usable images from the wet season took place during transitional periods, specifically early December and late March, rather than during the peak monsoon months, thereby distorting the seasonal comparison. We therefore interpret this pattern as an image artefact caused by the bias in imaging frequency and acknowledge that ground-based validation or microwave remote sensing would be necessary to accurately characterise seasonal thermal dynamics in tropical urban environments.

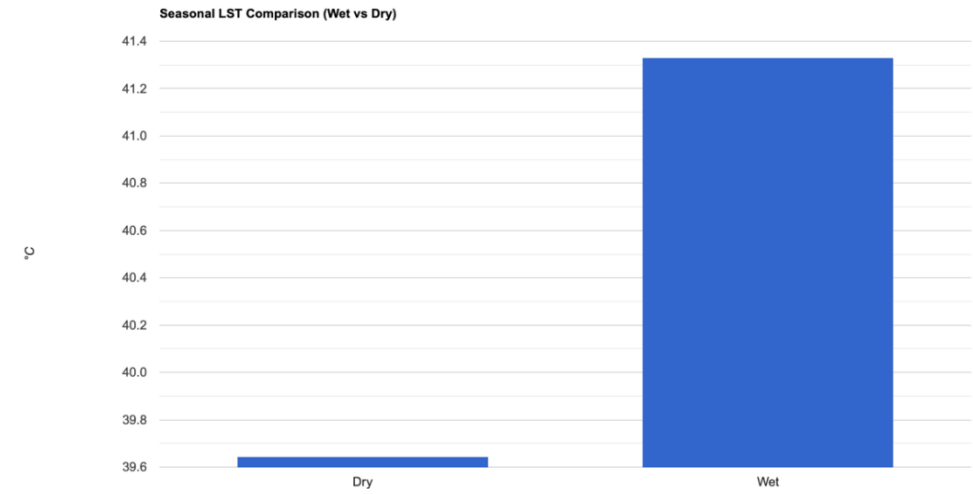

Figure 6. Seasonal LST comparison (Wet vs Dry)
Source: Processed from Landsat-8 (Collection 2 Level-2) imagery using Google Earth Engine

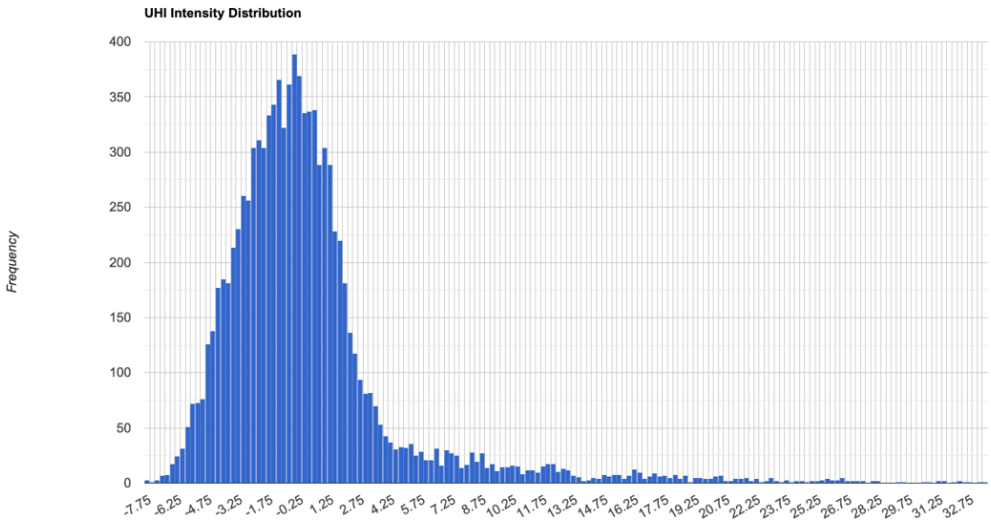

Figure 7. UHI intensity distribution
Source: Derived from mean LST values and NDBI classification using Landsat-8 and SRTM data in Google Earth Engine

Figure 6 shows seasonal LST comparison (Wet vs Dry). The intensity histogram of UHI indicates that the majority of locations experience an extra 0-2°C in temperature above rural reference points. Yet, certain areas document temperatures surpassing 10°C, indicating extreme heat build-up. The variations show that UHI in BSD is spatially uneven. Compact built-up areas and major transportation routes are frequently linked to higher intensity levels. In contrast, peripheral or greener areas experience lower UHI magnitudes. The disparities in heat exposure underscore the significance of urban design and green infrastructure in mitigating heat exposure.

Figure 7 shows UHI intensity distribution derived from mean LST values and NDBI classification. The combined results demonstrate that LST and UHI dynamics in BSD are influenced by both regional climate and local urbanization processes. Year-round mean annual LST has demonstrated a slight downward trend, yet extreme heatwaves continue to occur throughout the decade. Despite temporary declines, heat-related risks remain substantial. The persistence of extreme temperatures highlights that urban heat is a climatic issue as well as a structural outcome of land use patterns. Spatial planning, vegetation enhancement, and building regulations should therefore be integrated into policies. If these measures are not implemented, urban heat mitigation efforts will be restricted in scope and impact [30].

The ESI was created through the integration of three standardised indicators: LST (given a weight of 0.35), NO_2 concentrations (given a weight of 0.35), and flood susceptibility (given a weight of 0.30). This weighting scheme reflects the relative importance of thermal stress and air pollution in relation to their impact on human health, with flood risk considered as a further hydrological stress factor. The normalization process transformed each indicator into a scale of 0 to 1, thereby facilitating integration across different measurement units. The composite ESI theoretically ranges from 0 to 1, serving as a unified metric for evaluating environmental stress. The index calculation was conducted within Google Earth Engine, and spatial distribution patterns reveal higher values in regions where multiple stressors intersect, notably in densely populated areas with restricted green space availability. The ESI framework offers a methodological approach for pinpointing areas susceptible to multiple hazards that necessitate integrated environmental management.

This study's scope did not include detailed ESI mapping and population correlation analysis, yet the conceptual framework highlights the significance of integrated stress evaluation. The

approach suggests that concentrating on individual environmental stressors could lead to underestimating the overall effects in urban regions. Regions with moderate levels of individual stressors can still face high overall stress levels if thermal, atmospheric, and hydrological factors interact. The ESI methodology can assist urban planners in identifying areas where multiple environmental stressors intersect, enabling them to prioritise interventions accordingly. Future applications should integrate population density data and administrative boundaries to pinpoint high-risk communities and facilitate fair environmental decision-making processes. The framework's flexibility enables the adjustment of weights and the inclusion of extra stressors as data becomes available, thereby providing a scalable tool for tropical urban environmental assessment.

4.2 Air pollution trends and environmental stress interaction

The trend of NO_2 concentrations between 2019 and 2024 shows notable fluctuations over time. A marked decrease occurred in 2020, coinciding with mobility restrictions during the COVID-19 pandemic [31, 32]. The subsequent years saw a rebound in values, particularly in 2021 and 2023. This recovery demonstrates how economic and transport activities directly influence air quality. The rapid shift also highlights the vulnerability of suburban environments to policy and behavioral changes. These results provide a timely reminder that air pollution levels are highly sensitive to socio-economic conditions.

NO_2 levels averaged between 1.25×10^{-4} and 1.65×10^{-4} mol/m² during the observed time period. Compared to other metropolitan areas, these values indicate a significant environmental issue for BSD. The pattern is a reflection of emissions resulting from vehicles, industries, and household activities. The primary contributors to growth and increasing traffic density are infrastructural expansion and rising traffic levels. This trajectory aligns with BSD's status as a rapidly expanding suburban municipality. Unless action is taken, future levels may exceed the acceptable limits for human health.

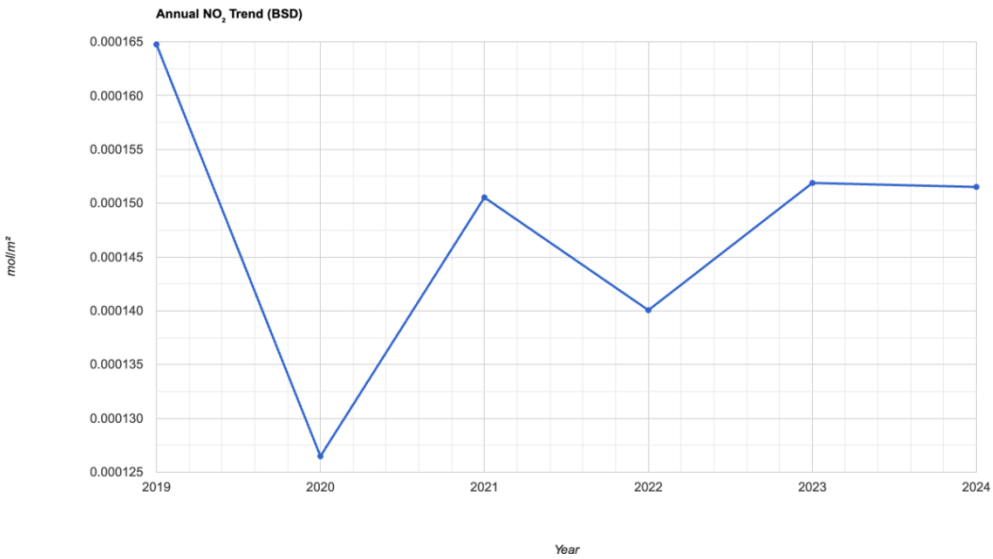

Figure 8. Annual NO_2 trend
Source: Processed from Sentinel-5P (TROPOMI) NO_2 column density data using Google Earth Engine

Figure 8 shows the annual NO_2 Trend. Although spatial distribution maps are not presented in this manuscript, our Google Earth Engine analysis revealed significant spatial heterogeneity in NO_2 concentrations across BSD City. Statistical analysis of pixel-level data showed that NO_2 values ranged from 0.95×10^{-4} mol/m² in peripheral green spaces to 2.15×10^{-4} mol/m² along major transportation corridors, indicating a 2.3-fold spatial variation. The coefficient of variation (CV = 0.42) confirms substantial spatial inequality in pollution exposure. Zonal statistics by land use category revealed the highest mean concentrations in commercial zones ($1.78 \pm 0.23 \times 10^{-4}$ mol/m²), followed by high-density residential areas ($1.52 \pm 0.19 \times 10^{-4}$ mol/m²), and the lowest in green spaces ($1.18 \pm 0.14 \times 10^{-4}$ mol/m²). Spatial autocorrelation analysis using Moran's I statistic ($I = 0.68$, $p < 0.001$) indicated significant clustering of pollution hotspots. While detailed mapping is beyond the scope of this study, these spatial statistics demonstrate that NO_2 pollution in BSD City is not uniformly distributed but follows predictable patterns associated with emission sources and urban morphology.

When LST and NO_2 are plotted together, their trends reveal contrasting behaviors. LST tends to fluctuate moderately, whereas NO_2 shows sharper year-to-year variability. This contrast suggests that the two indicators are controlled by different processes. LST is largely driven by climatic and physical parameters, while NO_2 is more responsive to human activity. The divergence further shows that environmental stress is multidimensional. Therefore, a combined approach is required to assess the urban atmosphere comprehensively [33].

Figure 9 shows the environmental trends of LST and NO_2. The interaction between heat and pollution intensifies health risks for urban residents [34]. Elevated LST increases the likelihood of heat-related illnesses and discomfort. Meanwhile, high NO_2 levels degrade respiratory health and contribute to atmospheric instability. Together, they impose a dual burden on vulnerable groups, including the elderly and outdoor workers. The compounding effect of these variables requires coordinated mitigation. Public health strategies must thus be designed with consideration of both pollutants and temperature stress.

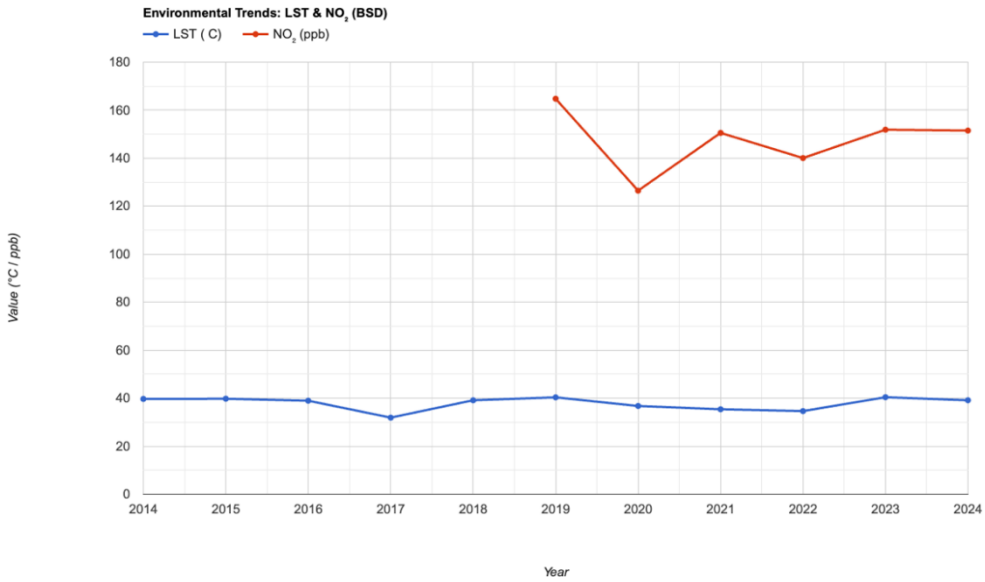

Figure 9. Environmental trends: LST and NO_2
Source: Combined analysis of Landsat-8 LST and Sentinel-5P NO_2 datasets using Google Earth Engine

In the composite Environmental Stress Index, LST and NO_2 are each assigned weights of 35%. This equal weighting reflects their comparable roles in shaping urban vulnerability. Flood susceptibility, which is weighted at 30%, completes the index structure. The index offers a holistic measure by integrating thermal, atmospheric, and hydrological risks [35-37]. It provides a more nuanced representation of environmental pressure than any single variable. Consequently, it supports evidence-based decision-making for urban sustainability [38-40].

Flood susceptibility mapping combined five critical factors with equal importance, each accounting for 0.2: normalised inverse slope, proximity to water bodies, wet season precipitation intensity, normalised inverse elevation, and historical water occurrence frequency. The composite flood susceptibility index varied between 0 and 1, and the natural breaks classification resulted in three risk categories: low (with FSI values below 0.35), moderate (with FSI values between 0.35 and 0.65), and high (with FSI values above 0.65). Regions with slopes of less than 2% and elevations below 30 meters exhibited the highest susceptibility values, especially when combined with proximity to drainage channels. Research showed that areas receiving more than 3000mm of rainfall annually during the wet season have a higher likelihood of flooding, as indicated by elevated flood susceptibility scores. Data from the JRC Global Surface Water revealed consistent inundation patterns in specific areas, which supports the flood susceptibility model. The analysis found spatial patterns of flood risk across BSD City, but detailed quantitative distributions need further ground validation.

A study of flood susceptibility in relation to land use patterns highlights key planning considerations. Residential areas in low-lying zones, especially those built on land previously used for farming or as wetlands, are more prone to flooding. Most commercial developments are primarily located on higher ground, implying that past flood risks were taken into consideration when choosing a site. Industrial zones exhibit varied levels of susceptibility, which are influenced by their individual locations and the drainage systems in place. Areas of greenery and unutilized land, despite exhibiting varying degrees of vulnerability to terrain features, are essential to water storage and percolation processes. Flood susceptibility in BSD City is not evenly dispersed throughout the area, but rather follows patterns linked to historical land-use decisions, geographical limitations, and proximity to water bodies. Future urban expansion plans should incorporate flood risk assessment to highlight its importance.

Overall, the combined findings indicate that BSD faces multiple and interconnected environmental threats. Surface heat, atmospheric pollutants, and flood risks together generate a layered stress landscape. Addressing these challenges requires interventions across different sectors simultaneously. Isolated measures, such as limiting traffic emissions, will have a limited impact without complementary spatial and hydrological strategies. Green infrastructure, emission control, and climate-adaptive planning must be pursued together. Only through integration can BSD reduce its environmental stress effectively.

5. CONCLUSION

This study demonstrates the complex spatiotemporal dynamics of urban environmental stress in BSD City through integrated remote sensing analysis. LST exhibits significant spatial heterogeneity with peak values reaching 45-46°C and UHI intensities exceeding 10°C in extreme hotspots, while counterintuitively showing marginally higher wet season values than dry season averages. NO_2 concentrations (2019-2024) reveal substantial temporal fluctuations with clear COVID-19 impacts in 2020, followed by recovery to concerning levels ($1.25\text{-}1.65 \times 10^{-4}$ mol/m²). The Environmental Stress Index successfully integrates thermal (35%), atmospheric (35%), and hydrological (30%) indicators, demonstrating that multidimensional assessment frameworks outperform single-variable approaches for comprehensive urban environmental evaluation.

The integrated remote sensing methodology advances urban environmental monitoring capabilities using freely available satellite datasets and provides a replicable framework for tropical metropolitan regions. The contrasting behaviors of climatically-driven LST and anthropogenically-responsive NO_2 confirm that environmental stressors require

differentiated mitigation strategies. Spatial heterogeneity patterns indicate that targeted interventions focusing on high-intensity zones can achieve greater effectiveness than uniform approaches, supporting evidence-based environmental management decisions in rapidly urbanizing areas.

Environmental stress mitigation requires coordinated, multi-sectoral interventions combining green infrastructure, emission controls, and climate-adaptive planning rather than isolated measures. Future research should focus on extended temporal analysis, ground-truth validation of satellite indicators, and predictive modeling incorporating urbanization scenarios. The urgency of implementing integrated strategies for sustainable urban development and public health protection in rapidly growing tropical cities cannot be overstated, particularly as BSD.

ACKNOWLEDGEMENT

The authors gratefully acknowledge Atma Jaya Catholic University of Indonesia for institutional support.

ATRIBUTION AND CLARIFICATION

The preparation of this manuscript utilized several supporting applications: Trinka for academic English grammar and writing style, Google Earth Engine for geospatial data processing, Napkin for visualization, QGIS for geographic information system analysis, Publish or Perish for citation metrics, and Mendeley for reference management. Literature sources were primarily obtained from Taylor & Francis Online (Tandfonline). All narrative content in this article has been thoroughly edited and adjusted in accordance with the editorial guidelines established by the journal. The authors take full responsibility for the accuracy and integrity of the content presented in this manuscript.

REFERENCES

[1] Manu, M., Li, J. (2025). Urban pavement crevices as microhabitats: Soil properties and spontaneous vegetation in roadside environments. International Journal of Sustainable Development & World Ecology, 32(6): 687-699. https://doi.org/10.1080/13504509.2025.2531435

[2] Cao, F., Li, J., Fu, X., Wu, G. (2020). Impacts of land conversion and management measures on net primary productivity in semi-arid grassland. Ecosystem Health and Sustainability, 6(1): 1749010. https://doi.org/10.1080/20964129.2020.1749010

[3] Mathew, A., Gokul, P.R., Raja Shekar, P., Arunab, K.S., Ghassan Abdo, H., Almohamad, H., Abdullah Al Dughairi, A. (2023). Air quality analysis and PM2.5 modelling using machine learning techniques: A study of Hyderabad city in India. Cogent Engineering, 10(1): 2243743. https://doi.org/10.1080/23311916.2023.2243743

[4] Iqbal, M., Susilo, B., Hizbaron, D.R. (2025). How local pollution and transboundary air pollution impact air quality in Jakarta? Papers in Applied Geography, 11(1): 49-62. https://doi.org/10.1080/23754931.2024.2399626

[5] Kamali Maskooni, E., Hashemi, H., Berndtsson, R., Daneshkar Arasteh, P., Kazemi, M. (2021). Impact of spatiotemporal land-use and land-cover changes on surface urban heat islands in a semiarid region using Landsat data. International Journal of Digital Earth, 14(2): 250-270. https://doi.org/10.1080/17538947.2020.1813210

[6] Guo, Y., Ren, Z., Dong, Y., Hu, N., et al. (2022). Strengthening of surface urban heat island effect driven primarily by urban size under rapid urbanization: National evidence from China. GIScience & Remote Sensing, 59(1): 2127-2143. https://doi.org/10.1080/15481603.2022.2147301

[7] Anupriya, R.S., Rubeena, T.A. (2025). Spatio-temporal urban land surface temperature variations and heat stress vulnerability index in Thiruvananthapuram city of Kerala, India. Geology, Ecology, and Landscapes, 9(1): 262-278. https://doi.org/10.1080/24749508.2023.2182088

[8] Guha, S., Govil, H., Besoya, M. (2020). An investigation on seasonal variability between LST and NDWI in an urban environment using Landsat satellite data. Geomatics, Natural Hazards and Risk, 11(1): 1319-1345. https://doi.org/10.1080/19475705.2020.1789762

[9] Ghimire, M., Regmi, T., Kayastha, S.P., Bhuiyan, C. (2023). Groundwater quality and community health risk in Lalitpur Metropolitan City, Nepal–A geospatial analysis. Geocarto International, 38(1): 2168069. https://doi.org/10.1080/10106049.2023.2168069

[10] Rabbani, M., Hossain, M.S., Islam, S.S., Roy, S.K., Islam, A., Mondal, I., Imam Saadi, S.M.A. (2024). Assessing thermal power effluent-induced air quality and associated environmental stress on Blumea lacera and Phyla nodiflora using chemometric, remote sensing and machine learning approach. Geology, Ecology, and Landscapes, pp. 1-19. https://doi.org/10.1080/24749508.2024.2430042

[11] Bahşi, K., Ustaoğlu, B., Aksoy, S., Sertel, E. (2023). Estimation of emissions from crop residue burning in Türkiye using remotely sensed data and the Google Earth Engine platform. Geocarto International, 38(1): 2157052. https://doi.org/10.1080/10106049.2022.2157052

[12] Han, H., Wichupankul, S., Cheng, X., Au, W.C.W., Tsang, K.F.N., Sangkaew, N. (2025). Influence of air pollution-related stressors and environmental-social responsibility on destination brand power (Chinese vs. Korean tourists). Journal of Travel & Tourism Marketing, 42(3): 356-377. https://doi.org/10.1080/10548408.2025.2470987

[13] Balgansuren, O., Arunotai, N. (2025). Contemporary urban environmental stresses and challenges on the pathway to sustainable development: Insights from an intersectional gender perspective in the ger communities of Ulaanbaatar, Mongolia. Local Environment, 30(11): 1420-1438. https://doi.org/10.1080/13549839.2025.2479001

[14] Fawakherji, M., Hashemi-Beni, L. (2025). Flood detection and mapping through multi-resolution sensor fusion: Integrating UAV optical imagery and satellite SAR data. Geomatics, Natural Hazards and Risk, 16(1): 2493225. https://doi.org/10.1080/19475705.2025.2493225

[15] Jiao, K., Yong, X., Mao, S., Chen, K. (2025). Analysis of the evolution and influencing factors of ecological environment quality after the transformation of resource-

exhausted cities based on GEE and RSEI: A case study of Xuzhou City, China. Journal of Asian Architecture and Building Engineering, 24(4): 2982-3000. https://doi.org/10.1080/13467581.2024.2358224
[16] Simon, O., Lyimo, J., Gwambene, B., Yamungu, N. (2024). Unveiling the transforming landscape: Exploring patterns and drivers of land use/land cover change in Dar es Salaam Metropolitan City, Tanzania. African Geographical Review, 43(7): 875-891. https://doi.org/10.1080/19376812.2024.2309405
[17] Shikwambana, L., Kganyago, M., Mbatha, N., Mhangara, P. (2024). First-time calculation of the spatial distribution of concentration and air quality index over South Africa using TROPOMI data. Journal of the Air & Waste Management Association, 74(8): 556-568. https://doi.org/10.1080/10962247.2024.2369751
[18] Almagbile, A., Hazaymeh, K. (2023). Spatiotemporal variability/stability analysis of NO_2, CO, and land surface temperature (LST) during COVID-19 lockdown in Amman city, Jordan. Geo-Spatial Information Science, 26(3): 540-557. https://doi.org/10.1080/10095020.2022.2066575
[19] Mondal, A., Guha, S., Kundu, S. (2021). Dynamic status of land surface temperature and spectral indices in Imphal city, India from 1991 to 2021. Geomatics, Natural Hazards and Risk, 12(1): 3265-3286. https://doi.org/10.1080/19475705.2021.2008023
[20] Khan, D., Bano, S., Khan, N. (2024). Spatio-temporal analysis of urbanization effects: Unravelling land use and land cover dynamics and their influence on land surface temperature in Aligarh City. Geology, Ecology, and Landscapes, 9(4): 1326-1350. https://doi.org/10.1080/24749508.2024.2409488
[21] Zheng, Y., Zhao, L., Lin, W., Ma, Q. (2025). Assessment of eco-environment quality using multi-source remote sensing data. International Journal of Sustainable Development & World Ecology, 32(2): 160-176. https://doi.org/10.1080/13504509.2024.2415977
[22] Bagherinia, M., Bodaghpour, S., Karimi, N., Ghasempour, F., Bilal, M., Mhawish, A. (2023). Spatio-temporal air quality assessment in Tehran, Iran, during the COVID-19 lockdown periods. Geocarto International, 38(1): 2169374. https://doi.org/10.1080/10106049.2023.2169374
[23] Roy, P., Chen, L.W.A., Linda, J., Khan, E., et al. (2024). Exploring dispersion modelling for resuspended pollen particles in a heterogeneous urban environment. International Journal of Environmental Studies, 81(4): 1698-1714. https://doi.org/10.1080/00207233.2024.2375856
[24] Arabameri, A., Seyed Danesh, A., Santosh, M., Cerda, A., Chandra Pal, S., et al. (2022). Flood susceptibility mapping using meta-heuristic algorithms. Geomatics, Natural Hazards and Risk, 13(1): 949-974. https://doi.org/10.1080/19475705.2022.2060138
[25] Mangkhaseum, S., Bhattarai, Y., Duwal, S., Hanazawa, A. (2024). Flood susceptibility mapping leveraging open-source remote-sensing data and machine learning approaches in Nam Ngum River Basin (NNRB), Lao PDR. Geomatics, Natural Hazards and Risk, 15(1): 2357650. https://doi.org/10.1080/19475705.2024.2357650
[26] Hanadé Houmma, I., Gadal, S., El Mansouri, L., Garba, M., Gbetkom, P.G., Mamane Barkawi, M.B., Hadria, R. (2023). A new multivariate agricultural drought composite index based on random forest algorithm and remote sensing data developed for Sahelian agrosystems. Geomatics, Natural Hazards and Risk, 14(1): 2223384. https://doi.org/10.1080/19475705.2023.2223384
[27] Kim, H.J., Rahman, M., Hammad, Z., Kim, H.S., Lee, S. J., Kim, T.E., Jung, S.H. (2025). Comprehensive analysis of coastal flood susceptibility, drought severity, and crop water stress using data fusion. Geomatics, Natural Hazards and Risk, 16(1): 2483809. https://doi.org/10.1080/19475705.2025.2483809
[28] Safaei, M., Kleinebecker, T., Große-Stoltenberg, A. (2023). Potential of the satellite-based dynamic habitat index (DHI) to capture changes in soil properties and drought conditions across Land Use/Land Cover types in a Central European landscape. Geocarto International, 38(1): 2292162. https://doi.org/10.1080/10106049.2023.2292162
[29] Aithal, B.H., Gupta, N., Dwivedi, G. (2024). Quantitative analysis of passive cooling measures in achieving a thermally comfortable urban environment. Geomatics, Natural Hazards and Risk, 15(1): 2347415. https://doi.org/10.1080/19475705.2024.2347415
[30] Huo, Z., Shang, Y., Zhou, S., Meng, M., Balsalobre Lorente, D., Ma, X. (2025). Monocentricity or polycentricity? The study on the enterprise environmental performance of urban spatial structure. Journal of the Asia Pacific Economy, 30(4): 1416-1446. https://doi.org/10.1080/13547860.2024.2370152
[31] Aboagye, E.M., Attobrah, J., Effah, N.A.A., Afrane, S., Mensah, F. (2021). "Fortune amidst misfortune": The impact of Covid-19 city lockdowns on air quality. Sustainable Environment, 7(1): 1885185. https://doi.org/10.1080/27658511.2021.1885185
[32] Ming, W., Zhou, Z., Ai, H., Bi, H., Zhong, Y. (2021). COVID-19 and air quality: Evidence from China. In Research on Pandemics, pp. 290-310. https://doi.org/10.1080/1540496X.2020.1790353
[33] Zubair, O.A. (2021). Investigating urban growth and the dynamics of urban land cover change using remote sensing data and landscape metrics. Papers in Applied Geography, 7(1): 67-81. https://doi.org/10.1080/23754931.2020.1817136
[34] Parisi, C.D.A., Kubota, T., Surahman, U. (2021). Affordable modifications for sustainable houses in urban informal settlements: A case study of Bandung, Indonesia. International Journal of Urban Sustainable Development, 13(3): 659-689. https://doi.org/10.1080/19463138.2021.1946544
[35] Correa, W.D.S.C., Aylas, G.Y.R., Santiago, A.M., do Vale, C.C., et al. (2024). Temporal and spatial urban heat islands in a coastal Brazilian area of tropical climate. Papers in Applied Geography, 10(2): 114-137. https://doi.org/10.1080/23754931.2024.2321561
[36] Mathew, A., Sarwesh, P., Khandelwal, S., Raja Shekar, P., et al. (2023). Thermal dynamics of Jaipur: Analyzing urban heat island effects using in-situ and remotely sensed data. Cogent Engineering, 10(2): 2269654. https://doi.org/10.1080/23311916.2023.2269654
[37] Zhou, M., Guo, H., Ouyang, X., Gunasekera, D., Sun, Z. (2025). Land surface temperature retrieval from SDGSAT-1: Assessment of different retrieval algorithms with different atmospheric reanalysis data. International Journal of Digital Earth, 18(1): 2492314.

https://doi.org/10.1080/17538947.2025.2492314
[38] Cai, A., Wang, J., MacLachlan, I., Zhu, L. (2020). Modeling the trade-offs between urban development and ecological process based on landscape multi-functionality and regional ecological networks. Journal of Environmental Planning and Management, 63(13): 2357-2379. https://doi.org/10.1080/09640568.2020.1723507
[39] Ali, M.B., Jamal, S. (2025). Modelling the present and future scenario of urban green space vulnerability using PSR based AHP and MLP models in a metropolitan city Kolkata Municipal Corporation. Geology, Ecology, and Landscapes, 9(3): 1141-1159. https://doi.org/10.1080/24749508.2024.2392377
[40] Verheij, J., Corrêa Nunes, M. (2021). Justice and power relations in urban greening: Can Lisbon's urban greening strategies lead to more environmental justice? Local Environment, 26(3): 329-346. https://doi.org/10.1080/13549839.2020.1801616